Air–Water Mass Transfer on a Stepped Waterway

L. Toombes[1] and H. Chanson[2]

Abstract: Stepped waterways are commonly used as river training, debris dam structures, storm water systems, and aeration cascades. The present study was focused on analysis of basic air–water flow properties on a low gradient stepped chute, combined with dissolved oxygen measurements. The oxygen aeration efficiency was found to be about 30% for 12 steps with a total drop in invert elevation of 1.4 m, nearly independently of the inflow conditions. Detailed air–water flow measurements, including void fraction, velocity, bubble count rate, and interface area, were used to integrate the mass transfer equation and to estimate the aeration potential of the waterway. Direct comparisons with dissolved oxygen measurements showed good agreement between the two methods.

CE Database subject headings: Aeration; Dissolved oxygen; Water quality; Waterways; Open channels.

Introduction

A stepped waterway is an open channel with the invert divided into a series of discrete drops or steps, the steps being horizontal, inclined upward or downward. Applications include river weirs, river training, debris dam structures, storm water systems, and aeration cascades. The influence of macroroughness and free-surface aeration on air–water gas transfer has been acknowledged for some time.

Recently, stepped cascades have been designed for the express purpose of water treatment. Fig. 1 illustrates a reoxygenation cascade: i.e., Station No. 1 (Chicago Torrence Ave. Station), one of five aeration cascades built along Chicago's Calumet Waterway to form the Sidestream Elevated Pool Aeration system. Stepped cascades are renowned for their high volume of air entrainment and high turbulence levels. Lower velocities are commonly observed compared to smooth chutes, giving the water a greater residence time on the cascade, consequently resulting in a greater mass of gas transferred. One of the earliest investigations into the aeration efficiency of stepped structures is that of Gameson (1957) (Table 1). Aeration efficiency in stepped chute models was measured by Tebbutt (1972) and Tebbutt et al. (1977) and Essery et al. (1978) (Table 1). Photographs by Tebbutt (1972) indicated however that little air entrainment occurred. The small dimensions of laboratory models used by Tebbutt and Essery induced most likely scale effects when extrapolated to larger structures (Chanson 2001). Several researchers investigated gas transfer at single drop structures (Table 2). Avery and Novak (1978) and Nakasone (1987) proposed correlations that were verified with prototype data.

In the present study, the writers investigated air–water mass transfer on a flat stepped waterway. New experiments were conducted in a near-full-scale facility. Air–water interfacial properties were systematically measured, and the results were combined with the mass transfer equation to predict the aeration efficiency of the chute. In parallel dissolved oxygen contents were recorded to assess its reoxygenation performances. Both sets of results were compared and the results emphasize the dominant aeration processes. It is the purpose of the paper to fill a void in this field, to compare aeration performances based upon basic multiphase flow properties with measured dissolved gas contents, and to present new compelling conclusions regarding air–water mass transfer in flat stepped waterways.

Air–Water Mass Transfer

The mass transfer rate of a chemical across an interface varies directly as the coefficient of molecular diffusion and the negative gradient of gas concentration. If the chemical of interest is volatile (e.g., oxygen), the transfer is controlled by the liquid phase and the gas transfer of the dissolved chemical across an air–water interface is rewritten usually as

$$\frac{\partial C_{\text{gas}}}{\partial t} = K_L a(C_{\text{SAT}} - C_{\text{gas}}) \tag{1}$$

where K_L=liquid film coefficient; a=specific surface area defined as the air–water interface area per unit volume of air and water; C_{gas}=local dissolved gas concentration; and C_{SAT}=concentration of dissolved gas in water at equilibrium (e.g., Gulliver 1990). Eq. (1) accounts for the variations of dissolved gas concentration in the cross section as well as the effects of hydrostatic pressure on the equilibrium concentration. Importantly it includes the effect of air bubble entrainment and the drastic increase in interfacial area in "white waters."

[1]Hydraulic Engineer, Connel Wagner, Spring Hill QLD 4000, Australia; formerly, Dept. of Civil Engineering, The Univ. of Queensland, Brisbane QLD 4072, Australia.

[2]Reader, Fluid Mechanics, Hydraulics and Environmental Engineering, Dept. of Civil Engineering, The Univ. of Queensland, Brisbane QLD 4072, Australia (corresponding author). E-mail: h.chanson@uq.edu.au

Fig. 1. Sidestream elevation pool aeration cascade (Chicago, Ill. 1988) (courtesy of The Metropolitan Water Reclamation District of Greater Chicago, with permission)

In open channel flows, Eq. (1) may be transformed as

$$\frac{\partial C_{gas}}{\partial x} = K_L V_{mean} a_{mean} (C_{SAT} - C_{gas}) \qquad (2)$$

where x=streamwise coordinate; a_{mean}=cross-section average specific interface area; and V_{mean}=average velocity defined, respectively, as

$$a_{mean} = \frac{1}{W z_{90}} \int_{-W/2}^{+W/2} \int_{0}^{z_{90}} dz\, dy \qquad (3)$$

$$V_{mean} = \frac{1}{W z_{90}} \int_{-W/2}^{+W/2} \int_{0}^{z_{90}} V dz\, dy \qquad (4)$$

W=channel width; z=vertical coordinate; y=transverse coordinate measured from the centerline; z_{90}=characteristic distance where $C=0.90$; C=void fraction (i.e., volume of undissolved gas per unit volume of air–water mixture); and V=local air–water velocity.

Eqs. (1) and (2) demonstrate that the rate of gas transfer is proportional to the surface area of the air–water interface and the dissolved gas concentration deficit. Ideal conditions for gas transfer are highly aerated turbulent flows with large numbers of small air bubbles, hence very large specific interface area, and relatively slow mean velocities.

Experimental Facilities

New experiments were performed in two open channels (Table 3). The first flume was 0.5 m wide and equipped with 12 identical 0.143 m high 2.4 m long steps followed by a 1.14 m high free overfall (Fig. 2). The second channel was 0.25 m wide, 3.2 m long, equipped with a single 0.143 m high drop and ending with a free overfall. Both channels had supercritical inflow conditions: $2 \leqslant F_0 \leqslant 10$, where F_0=approach flow Froude number. For all experiments, nappe ventilation by sidewall splitters was provided at the first drop.

Instrumentation

The water flow rates were measured with a V-notch weir in the 0.25 m wide channel and with a Dall tube flowmeter for the 0.5 m wide flume. The accuracy on discharge measurements was about 2%. Clear-water flow depths and velocities were measured with a point gage and a Prandtl–Pitot tube ($\varnothing=3.3$ mm), respectively.

Dissolved oxygen contents were recorded using a TPS 90FLMV microprocessor field analyzer. The system recorded dissolved oxygen content, conductivity, linearized salinity, pH, and temperature. Automatic compensation for temperature and water salinity was included when measuring dissolved oxygen.

Air–water flow properties were measured using a single-tip conductivity probe ($\varnothing=0.35$ mm) in the wide channel ($W=0.5$ m) and a double-tip conductivity probe ($\varnothing=0.025$ mm) in the narrow flume ($W=0.25$ m). Both probes are phase-detection intrusive probes designed to pierce incoming bubbles. The basic features of each type of probe were discussed in Chanson (1997, 2002) and Toombes (2002). The probes were developed at the Univ. of Queensland and excited by an air bubble detector (AS25240). The resistivity probe signals were scanned at 8 kHz for 180 s and 40 kHz for 40 s for the single-tip and double-tip resistivity probes, respectively. The translation of the probes in the direction normal to the channel invert was controlled by a fine adjustment travelling mechanism connected to a MitutoyoTM digimatic scale unit (Reference No. 572-503). The error on the vertical position of the probe was less than $\Delta z < 0.025$ mm. The system (probe and traveling mechanism) was mounted on a trolley system. The accuracy on the longitudinal position of the probe was estimated as $\Delta x < 0.5$ cm. The accuracy on the transverse position of the probe was estimated as $\Delta y < 0.5$ mm. Further information and details were provided in Toombes (2002).

Air–Water Interfacial Area Measurements

Air–water flow measurements were systematically conducted at several cross sections in the free jet, next to nappe impact and in the downstream flow region. At each cross section, vertical

Table 1. Summary of Gas Transfer Experiments on Stepped Chutes

Reference	Slope (%)	q_w ($\times 10^{-3}$ m$_2$/s)	H (m)	d_c/h	Remarks
Gameson (1957)					$H_{\text{dam}}=0.9$–2.2 m
Barrett et al. (1960)					$H_{\text{dam}}=2.6$ m, $W=60$ m, $T=25°$C. Skimming flow
Tebbutt (1972)	35.5	0.28–1.53	0.05	0.002–0.124	
	45	0.56–13.0	0.073	0.043–0.36	$H_{\text{dam}}=1.8$ m, $W=0.3$ m
	45	0.56–13.0	0.127 and 0.254	0.0125–0.206	$H_{\text{dam}}=1.8$ m, $W=0.3$ m
Tebbutt et al. (1977)	11.3, 21.8, and 45	77–965	0.05	1.69–9.12	$H_{\text{dam}}=2$ m, $W=0.15$ m $13<T<30°$C
			0.1	0.85–4.56	
			0.25	0.34–1.82	
			0.5	0.17–0.91	
Essery et al. (1978)	21.8, 45	10–145	0.025–0.5	0.05–2.6	$H_{\text{dam}}=2.0$ m, $W=0.15$ m. Horizontal and inclined upward steps. $\alpha_s=0,10,20°$. $T=20°$C
	11.3				$H_{\text{dam}}=1.0$ m
Butts and Evans (1983)			0.3048		$H_{\text{dam}}=1.22$ m. North Aurora and Montgomery dams.
			0.3048		$H_{\text{dam}}=2.13$ m. McHenry dam.

Note: d_c=critical depth; H=total head; H_{dam}=dam height; h=step height; q_w=discharge per unit width; T=temperature; and W=channel width.

profiles were recorded between $z=0$ (i.e., step invert) and the upper "free surface" defined as z_{90} at several transverse positions, although air–water flow measurements in the larger Channel 1 were performed predominantly on the centerline.

The basic outputs of single-tip and double-tip probes are the void fraction and bubble count rate distributions. The Void Fraction C is the proportion of time that the probe tip is in the air. The bubble count rate F is the number of bubbles impacting the probe tip. A double-tip probe design provides additionally the air–water velocity distributions. The local time-averaged air–water velocity is deduced from a cross-correlation technique between leading and trailing tip signals.

For an air–water mixture consisting of spherical air bubbles of uniform diameter ϕ_a, the specific interface area may be estimated as

$$a = \frac{6C}{\phi_a} \tag{5}$$

Intrusive probes, such as the conductivity probes used in the current study, do not measure bubble diameter but bubble chord length. At a given location, air bubbles and water droplets are of nonuniform size and unlikely to be spherical, except possibly at very low void fractions (i.e., $C<0.1$). In a complex bubbly flow region, the specific interface area is simply proportional to the number of air–water interfaces per unit length of air–water mixture

$$a = n\frac{2F}{V} \tag{6a}$$

where the constant n=function of the shape of the bubbles. For spherical and ellipsoidal air bubbles and water droplets, $n=2$. For simplicity, and in the absence of evidence to the contrary, a value of $n=2$ was used across the complete section, allowing Eq. (6a) to be written as

$$a = \frac{4F}{V} \tag{6b}$$

Although the exact shape of bubbles (and hence n) is unknown, experimental analysis presented in Chanson (1997) indicated that Eq. (6b) gave a reasonable approximation of the air–water interface area.

Reoxygenation Measurements

The oxygenation performances of the multistep cascade were measured in situ. Total aeration of the chute system consisted primarily of two processes: aeration on the stepped cascade, and aeration by plunging jet where the water at the end of the cascade reentered the pool in the storage tank (Fig. 2). Prior to each experiment, the water in the pit tank was deoxygenated with sodium sulphite ($NaSO_3$). Then the cascade was operated and the dissolved oxygen (DO) content of the water was recorded at the downstream of the chute, in the pit immediately downstream of the overfall, and immediately upstream of the pump intake. The stepped waterway aeration efficiency was estimated as

$$E_{\text{cascade}} = \frac{E_{\text{system}} - E_{\text{overfall}}}{1 - E_{\text{overfall}}} \tag{7}$$

where E=aeration efficiency defined as

$$E = \frac{C_{\text{DS}} - C_{\text{US}}}{C_{\text{SAT}} - C_{\text{US}}} \tag{8}$$

C_{SAT}=saturation dissolved gas concentration; C_{US} and C_{DS}=upstream and downstream dissolved gas concentrations, respectively; E_{system}=overall efficiency of the entire system; and E_{overfall}=aeration efficiency of the overfall. Herein all results are presented in terms of aeration efficiency for dissolved oxygen at 20°C and standard pressure.

Table 2. Summary of Gas Transfer Experiments at Free Overfalls

Reference	q_w ($\times 10^{-3}$ m^2/s)	Fall height (m)	Remarks
DSIR (1957)		0.61 and 1.52	Model data, $0 < d_t < 0.30$ m
Mastropiertro (1968)		1.22–4.6	Prototype data, $10° < T < 25°$C
Holler (1971)		3.7,8.4,10.7	Prototype data Tailwater depths < 4.9 m
Apted and Novak (1973)	6.2–21	1.15	Model data, $W = 0.01$ m $0.05 < d_t < 0.45$ m
Department of Environment (1973)		0.15,0.51,1.52,3.05	Model data, $0 < d_t < 0.45$
Foree (1976)	$Q_w = 0.057 - 0.4$ m^3/s	0.79–7.3	Prototype data $17 < T < 24°$C
Avery and Novak (1978)	3–50	0.25–2.1	Rectangular jets. Model data $W = 0.1, 0.22, 0.3$ m
Nakasone (1987)	11–741 27–7,800	0.24–1.98 152–5.8	Weir, model data, $W = 0.2, 0.3$ m Weir, prototype data
Watson et al. (1998)	45.8–196 45.9–93.3	0.173–0.750 0.422–0.673	Rought weir model, $0.138 < d_t < 0.671$ m Smooth weir model, $0.201 < d_t < 0.404$ m

Note: DSIR = Department of Scientific and Industrial Research and d_t = tailwater depth.

Measurements of oxygenation performance of the cascade were complicated by a few problems, including mixing in the pit tank and a "dead-end" region of the pit tank (Fig. 2, left of pump). Preliminary tests showed that the DO content in this region remains negligible even when the rest of the water has been reoxygenated, indicating that there was little mixing occurring between the water cycling through the system and the water in this region of the tank.

Experimental Results: (1) Interfacial Aeration

Different mechanisms were observed to contribute to air entrainment in nappe flows down the stepped waterway (Fig. 3). Basic observations suggested that these may include: (1) free-surface aeration at the jet interfaces; (2) air entrainment by the plunging jet where the free-falling nappe impacts into the recirculating pool; (3) singular aeration at the hydraulic jump occurring

Table 3. Experimental Flow Conditions

R	h (m)	W (m)	d_o (m)	q_w (m^2/s)	F_o	d_c/h	Comments
Channel 1	0.1433	0.5					Twelve identical horizontal timber steps. Sidewall offset for nappe ventilation at first drop.
			0.030	0.080	4.9	0.6	
			0.030	0.110	6.8	0.75	
			0.030	0.150	9.2	0.92	
Channel 2	0.1433	0.25					Single horizontal perspex step and glass flume. Sidewall offset (6.5 mm on each side) for nappe ventilation at drop.
			0.031	0.084	4.9	0.62	Run DT1
			0.029	0.097	6.3	0.69	Run DT2
			0.030	0.111	6.8	0.75	Run DT3
			0.024	0.087	7.5	0.64	Run DT4
			0.040	0.143	5.7	0.89	Run DT5

Note: d_c = critical flow depth.; d_o = approach flow depth; F_o = inflow Froude number; h = step height; R = Reynolds number defined in terms of hydraulic diameter; and W = channel width.
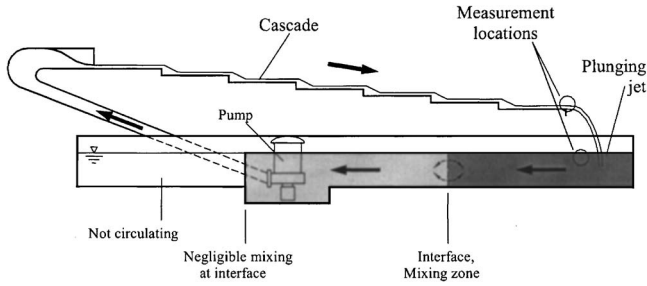
Fig. 2. Sketch of multistepped waterway (not to scale; number of steps reduced for clarity)

Fig. 3. Aeration mechanisms typical of nappe flow regime with hydraulic jump

downstream of the nappe impact, or, if there is no hydraulic jump; and (4) flow fragmentation and pulverization at the free surface of the supercritical flow downstream of nappe impact. In the present study, all investigated flow conditions corresponded to a nappe flow regime without hydraulic jump as defined by Chanson (2001). That is, the flow downstream of nappe impact was supercritical up to the next step brink. Typical vertical profiles of specific interface area on the single step channel are shown in Fig. 4 together with the corresponding distributions
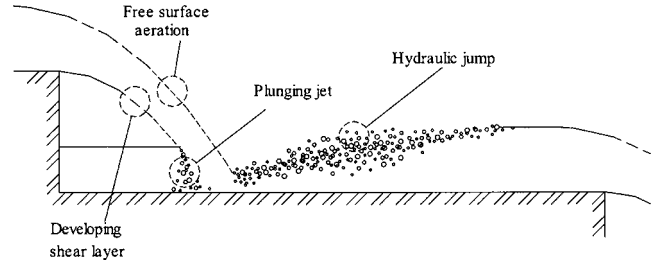
of velocity and bubble count rate. The data are presented in dimensionless form as V/V_0, a d_0 and $F d_0/V_0$, where d_0 is the centerline clearwater flow depth measured 0.15 m upstream of the drop, $V_0=q_w/d_0$, q_w is the water discharge per unit width, while $X=x/d_0$, $Y=2y/W$, and $Z=z/d_0$ are the dimensionless longitudinal, transverse, and perpendicular distances measured relative to the upstream step edge, the channel centerline, and the step invert, respectively.
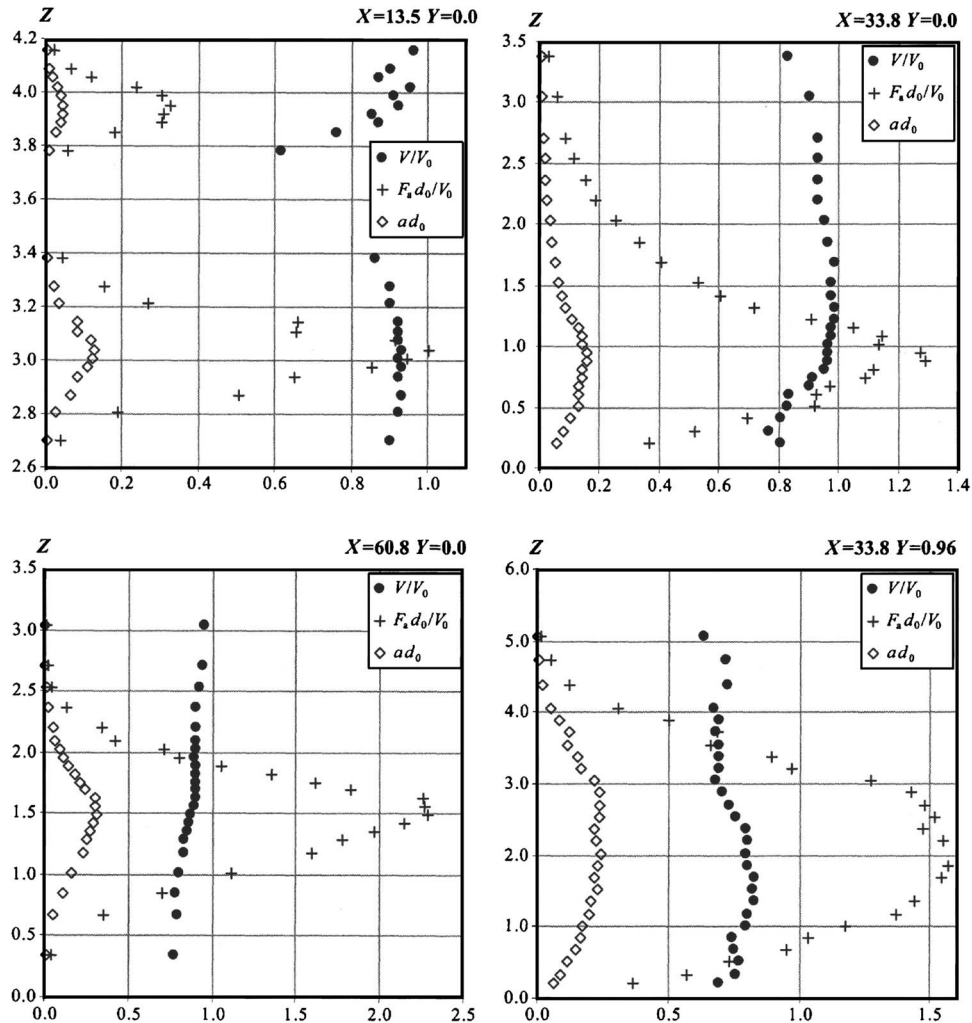

Fig. 4. Typical dimensionless profiles of velocity, bubble frequency, and specific interface area (Channel 2, $q_w=0.111$ m^2/s, $W=0.25$ m, m, $d_0=29.6$ mm, $V_0=3.75$ m/s): (a) free-falling nappe ($x=0.40$ m); (b) Centerline spray region ($x=1.0$ m); (c) Centerline downstream ($x=1.80$ m); and (d) sidewall standing wave ($x=1.0$ m)

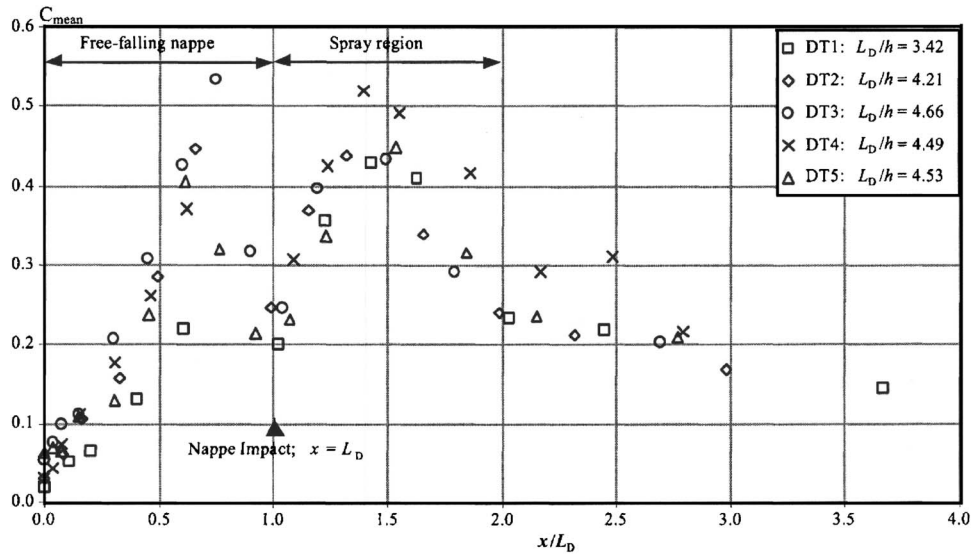**Fig. 5.** Longitudinal distributions of cross-sectional mean air concentration in single-step model: (DT1) $q_w = 0.084$ m²/s; (DT2) $q_w = 0.097$ m²/s; (DT3) $q_w = 0.111$ m²/s; (DT4) $q_w = 0.087$ m²/s; and (DT4) $q_w = 0.143$ m²/s

At a given location, the mean void fraction in the flow cross section is defined at

$$C_{mean} = \frac{1}{W z_{90}} \int_{-W/2}^{+W/2} \int_{0}^{z_{90}} C \, dz \, dy \qquad (9)$$

Variations of cross-section mean void fraction along a single step are shown in Fig. 5 where x=distance downstream of the step brink and L_D=measured drop length of the free-falling nappe. Since the jet impact length L_D is a function of the flow rate, dimensionless values of the jet impact length L_D/h are reported in the figure legend. Downstream of nappe impact the data have a similar dimensionless shape, being largely independent of upstream flow depth, velocity, and void fraction (Fig. 5). Only one experiment (Run DT4) with the shallowest flow depth exhibited consistently slightly higher aeration than other results. In the single-step channel, the cross-sectional averaged void fraction was relatively small upstream of the step brink (i.e., $C_{mean} < 6\%$). The void fraction rapidly increased along the free-falling nappe, reaching around 50% before nappe impact for some experiments. Investigation of upper and lower nappe interfacial aeration showed that the increase was largely caused by interfacial air entrainment at the lower jet interface. The mean void fraction at nappe impact was less than in the impacting jet, possibly because of the presence of the recirculating pool beneath the nappe. Maximum mean void fractions were observed in the spray region, with decreasing mean void fraction with increasing distance from nappe impact. These findings were consistent with those observed on the larger multistep channel.

Cross-sectional average specific interface area measurements [Eqs. (3) and (6)] are presented in Fig. 6, for the same data set as shown in Fig. 5. Overall results suggested that the maximum mean specific interface area occurred within the spray region downstream of nappe impact, and that its dimensionless value was independent of the inflow conditions. The total interface area available for mass transfer on the entire step was however a complex function of inflow properties, because the lengths of both free-falling nappe and highly aerated "spray region" (Fig. 6) varied relative to the length of the step.

Downstream of the spray region (Fig. 6, $x/L_D > 1.5$), the average specific interface area decreased almost linearly with distance from nappe impact. The data downstream of nappe impact were best correlated by

$$a_{mean}(h + d_0) = 54 \left(\frac{x}{L_D} \right)^{0.85} 2^{-x/L_D} \quad (x/L_D > 1) \qquad (10)$$

where $(h + d_0)$=elevation of the upstream water depth relative to the downstream invert. Eq. (10) is compared with experimental data in Fig. 6.

Calculated Aeration Efficiency

The aeration efficiency of a single step is the aggregate of the contribution of each aeration mechanism (Fig. 3)

$$E_{STEP} = 1 - (1 - E_{JET})(1 - E_{PJ})(1 - E_{HJ})(1 - E_{FS}) \qquad (11)$$

where the subscripts JET, PJ, HJ, and FS refer to the contributions from the upper and lower interfaces of the free-falling jet, the plunging jet, the hydraulic jump, and the free-surface aeration in the downstream flow, respectively. The aeration efficiency for a cascade of N steps may be expressed in terms of the aeration efficiency at each step

$$E_{cascade} = 1 - (1 - E_1)(1 - E_2) \cdots (1 - E_N) \qquad (12)$$

where E_i=aeration efficiency for the ith step.

For each channel, the aeration efficiency of a single step was estimated by integrating Eq. (2) in the streamwise direction x along the step, using the cross-sectional averaged air–water flow properties, namely flow velocity V_{mean}, the specific interface area a_{mean}, and the dissolved gas concentration C_{gas}. The coefficient of mass transfer K_L was assumed constant independently of bubble size and flow conditions as demonstrated by Kawase and Moo-Young (1992) for turbulent shear flows, and the dissolved gas saturation concentration C_{SAT} was assumed constant. For the single-step channel, aeration efficiency for oxygen $E(O_2)$ is shown in Fig. 7. Calculations were conducted for a temperature of 20°C and pressure of 1 atm, and based upon measured
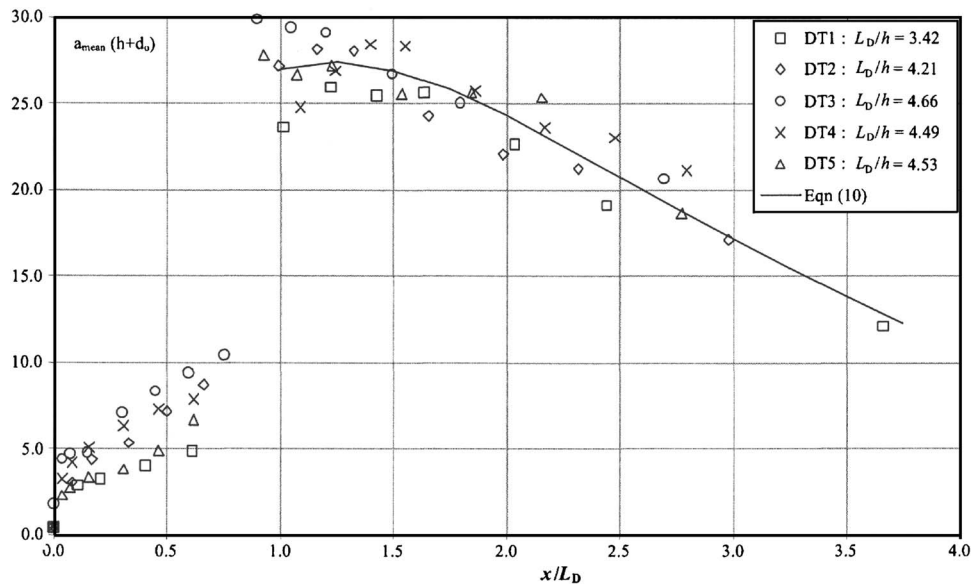
Fig. 6. Longitudinal distribution of cross-sectional average specific interface area in single-step model: (DT1) q_w=0.084 m²/s; (DT2) q_w=0.097 m²/s; (DT3) q_w=0.111 m²/s; (DT4) q_w=0.087 m²/s; and (DT4) q_w=0.143 m²/s [comparison with Eq. (10)]

cross-sectional averaged velocity and specific interface area. The results showed a consistent trend. Limited aeration occurred in the free-falling nappe because of the relatively small specific interface area. Downstream of nappe impact, the rate of aeration increased rapidly in the highly aerated spray region, while it decreased gradually near the downstream end as the specific interface area decreased. For the investigated flow conditions in the single-drop channel (Table 3), the aeration efficiency along the step may be approximated as Single-step

$$E = 0.02 \exp\left(-2.9\frac{L_D}{x}\right)\mathsf{F}_0^{0.75} \qquad (13)$$

where F_0=inflow Froude number. Eq. (13) is compared with the data in Fig. 7.

In the single-step channel, the inflow configuration was characterized by relatively little free-surface aeration, similar to the flow at the first drop of the multistepped channel. On the subsequent steps, however, the flow was affected by a number of conflicting characteristics that acted to increase or decrease the aeration potential. Centerline single-tip conductivity probe measurements were integrated along the stepped cascade, and calculated oxygen aeration efficiencies achieved by individual steps are shown in Fig. 8. That is, each data point represents the aeration efficiency over a single step, not the cumulative efficiency of the cascade to that point. The efficiency of each step is plotted as a function of dimensionless distance x/L_{casc}, where x is the distance between the flume inlet and the downstream end of that step, and L_{casc} is the length of the cascade. The results highlight the variation in aeration efficiency of individual steps along the cascade, and they are compared with single step model results.

Discussion

Despite comparable flow rates and geometry, the order of magnitude of calculated aeration efficiencies, was approximately twice on the single-step channel as that observed at the first abrupt drop (Step 2) of the multistep model (Fig. 8, x/L_{casc}=0.2). There were two basic differences between the single-step and multistep

cascade experiments. First the multistep cascade experiments were obtained using a sturdy single-tip conductivity probe (sensor size $\varnothing$=0.35 mm), as opposed to the double-tip conductivity probe ($\varnothing$=0.025 mm) used in the single-step flume. The double-tip probe had a significantly smaller sensor size and was consequentially capable of detecting much smaller bubbles. Although the contribution of these small bubbles to the void fraction may be small, they had a significant influence on specific interface area. The findings were consistent with the experiments of Chanson and Toombes (2002) on a 22° stepped chute, in which they systematically compared the performances of sturdy and fine conductivity probes. Second the results for the multistepped channel were extrapolated from centerline data. In the single-step flume, the result were based upon three-dimensional measurements, and they indicated that three-dimensional air–water flow patterns, such as observed sidewall standing wave and shock waves, had some influence on the average specific interface area and velocity at a cross section.
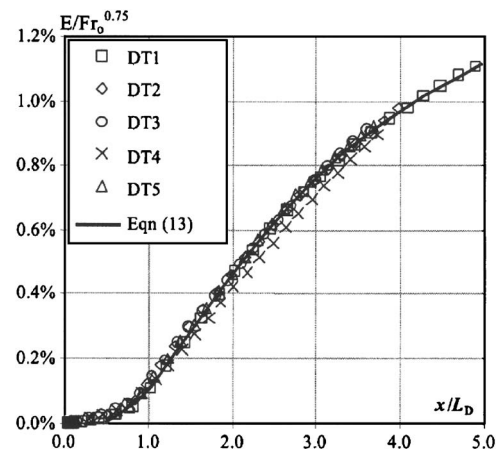

Fig. 7. Modified aeration efficiency $E/\mathsf{F}_0^{0.75}$ at 20°C of single-step model as function of distance downstream from step brink—comparison between calculations and Eq. (13)
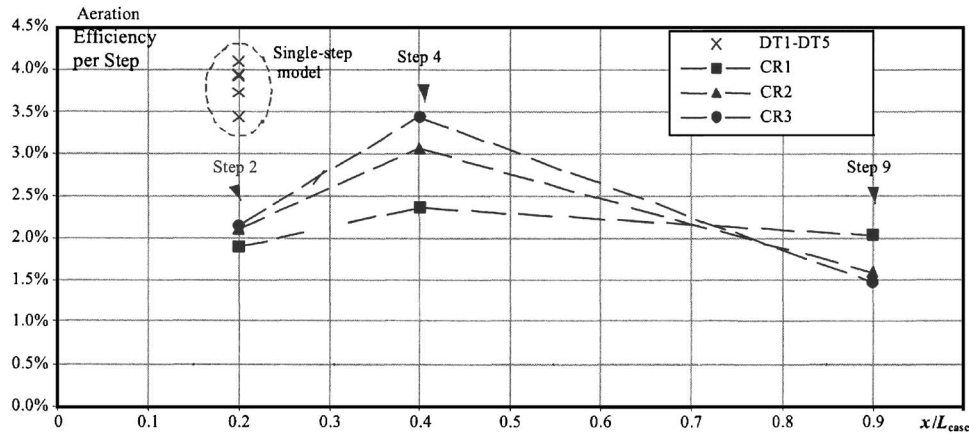
Fig. 8. Calculated oxygen aeration efficiency at 20°C of individual steps along multistep cascade—comparison with single-drop channel: L_{casc}=24 m; (Run CR1) q_w=0.08 m²/s; (Run CR2) q_w=0.11 m²/s; and (Run CR3) q_w=0.15 m²/s

Experimental Results: (2) Dissolved Oxygen Measurements

Multistepped Cascade Oxygenation

Reoxygenation performances of the multistepped chute are presented in Fig. 9, based upon dissolved oxygen measurements. The full data set is presented in Table 4. Aeration efficiency of the complete system (cascade and overfall) is also shown for completeness. The data are presented as functions of the inflow Froude number F_0.

The total aeration efficiency of the stepped cascade plus free-overall system ranged typically from 75 down to 60% for upstream Froude numbers between 2 and 10. The aeration efficiency steadily decreased with increasing Froude number. For the present investigation, the total aeration of stepped chute plus free-overfall was best correlated by total aeration efficiency

$$E = 0.77 \exp(- 0.021 F_0) \qquad (14)$$

where F_0=inflow Froude number. Eq. (14) expresses the reoxygenation performance as a function of the inflow Froude number.

The aeration efficiency of the stepped chute (only) is compared with calculated aeration efficiencies in Fig. 9. With the exception of the lowest flow rate, the aeration efficiency for dissolved oxygen of the multistepped channel was relatively constant: i.e., $E(O_2) \approx 30\%$ for $3 < F_0 < 10$. The data showed no consistent variation with inflow Froude number F_0 nor dimensionless flow rate d_c/h. Calculations based upon double-tip conductivity probe data, measured in the single-drop channel, predicted a similar aeration efficiency of $E(O_2) \approx 30\%$ for $5.0 < F_0 < 7.6$. Overall, these results showed an excellent agreement with the dissolved oxygen measurements (Fig. 9).

The extrapolation of the double-tip probe data was conducted for the 12 steps cascade assuming that the aeration efficiency of each step was a constant equal to the calculated aeration efficiency in the single step channel. Note that calculations based upon single-tip conductivity probe data resulted in lower estimates: $E(O_2) \approx 19\%$ (Fig. 9). As shown in Fig. 8 for x/L_{casc}=0.2, the single-tip conductivity probe data appeared to underestimate the aeration efficiency of a single step. Basically the single-tip conductivity probe underestimated bubble frequency and specific interface area, hence yielding conservative aeration efficiency estimates. It is believed that

bubbles and droplets with chord sizes between about 0.025 and 0.35 mm, detected by the dual-tip probe and not by the single-tip probe, had a significant contribution to the specific interface area, hence to the air–water mass transfer. Based upon the present results, it is believed that a minimum sensor resolution of 0.1–0.15 mm was required for an accurate prediction.

Oxygenation at Free Overfall

The oxygen aeration efficiency of the free overall at the downstream end of the multistepped cascade was recorded for a range of flow conditions. Some results are presented in Fig. 10 as a function of the Froude number at the overfall brink. It must be emphasised that the data are the only data set on oxygen transfer at abrupt drops with supercritical inflow conditions.

The results were compared with a dozen of empirical correlations (Toombes 2002). Despite some data scatter, the trend was best fitted by the correlations of Nakasone (1987); Avery and Novak (1978); and Foree (1976). For the present study, the correlation of Nakasone was found to fit best the data trend. Note that the majority of these studies were conducted using subcritical inflow conditions, whereas the flow upstream of the overfall for the current study was supercritical.
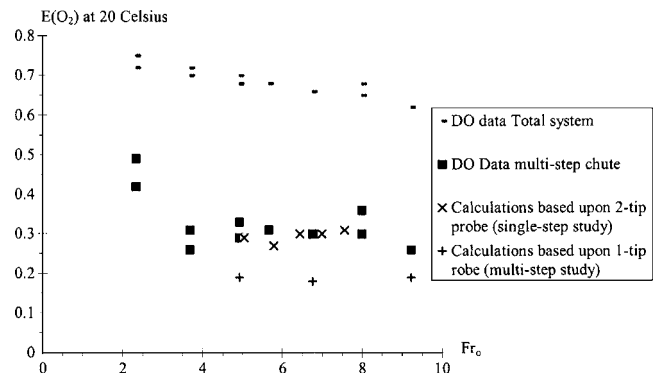

Fig. 9. Aeration efficiency at 20°C of multistepped channel as a function of inflow Froude number F_0: dissolved oxygen measurements (total system and stepped chute only) and calculations based upon measured interfacial areas (stepped chute only)

Table 4. Aeration Efficiency of Multistepped Waterway Based upon Dissolved Oxygen Measurements

q_w (m²/s)	F_0	$E(O_2)$[a] Total system (stepped channel+overfall)	$E(O_2)$ Stepped channel
0.038	2.34	0.75	0.49
0.038	2.34	0.72	0.42
0.60	3.69	0.72	0.31
0.60	3.69	0.70	0.26
0.080	4.92	0.70	0.33
0.080	4.92	0.68	0.29
0.092	5.66	0.68	0.31
0.092	5.66	0.68	0.31
0.110	6.76	0.66	0.30
0.130	7.99	0.68	0.36
0.130	7.99	0.65	0.30
0.150	9.22	0.62	0.26

[a]E=measured aeration efficiency, reported for 20°C and standard pressure using the temperature dependence relationship of APHA/AWWA/WPCF (1989)

Fig. 10. Aeration efficiency at 20°C of free overfall at downstream end of multistepped channel, based upon dissolved oxygen measurements, as function of overfall brink Froude number

Discussion

Aeration performances based upon measured air–water flow properties (i.e., bubble frequency, void fraction, velocity) were found to give an excellent estimate of experimentally measured aeration efficiency (Fig. 9). The experimental results suggested that the aeration efficiency on a stepped chute is a complex function of the step geometry (height, length) and inflow conditions (depth, velocity, initial level of air entrainment). Stepped waterway flows are characterized by a high level of turbulence, which helps to distribute the solute (i.e., constantly renew the fluid at the boundary) and maintain maximum concentration gradient at the surface, while a high level of air entrainment increases the interface area available for mass transfer.

The gradient of the chute has some influence on the chute performances. An increasing chute slope for a constant step height can increase the aeration efficiency per unit of streamwise length because there are more drops per unit length. But it may decrease the aeration efficiency per unit height. Indeed the aeration efficiency of a single step drop will be reduced as the water spends less time on the step. This simple reasoning implies that shorter step lengths are less economically efficient, since height is congruent with energy and power, whether it be to pump the water to the head of the cascade [e.g., Calumet Waterway cascades, Chicago, Ill. (Fig. 1)], or a loss of potential from an upstream dam (e.g., Petit-Saut Dam, Sinnamary River, French Guyana).

The multistepped channel results were further compared with calculated aeration efficiency for the same chute equipped with a smooth invert (Chanson 1997). The latter data were calculated based upon double-tip conductivity probe data. Bubble frequencies, interface areas, and aeration efficiency were comparable to the current study. All flow conditions being equal, the stepped waterway was clearly significantly more efficient than the smooth chute, with an aeration efficiency for oxygen of about $E \approx 30\%$ by the end of the cascade compared to $E \approx 3.5\%$ on the 24 m long smooth chute.
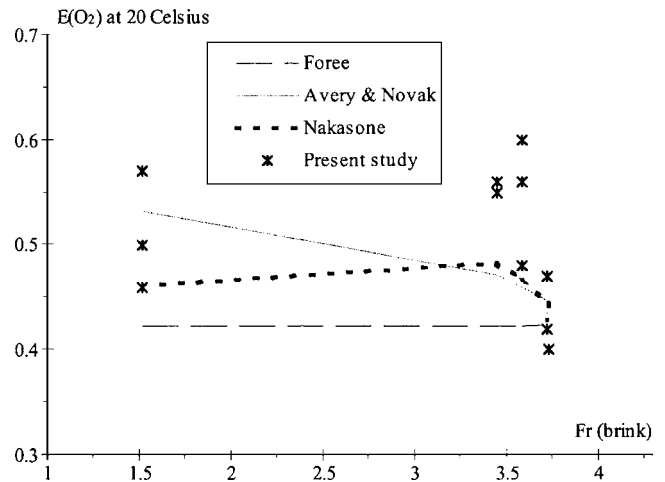
Conclusion

Stepped waterways are recognized for both energy dissipation and aeration potential. The present study was focused on analysis of basic air–water flow properties on a low gradient stepped cascade, combined with dissolved oxygen measurements. Overall the oxygen aeration efficiency was found to be about 30% for a total drop in invert elevation of 1.4 m, and the result was nearly independent of the flow conditions for the range of the investigations (Table 3).

Detailed air–water flow measurements, including void fraction, velocity, bubble count rate, and interface area, were used to estimate the aeration potential of the stepped waterway based upon the basic mass transfer equation. Direct comparisons between DO measurements and numerical integration of the mass transfer equation, showed good agreement between the two methods. The results supported the use of the mass transfer equation to calculate the aeration efficiency of stepped cascades and other structures using measured air–water flow properties. However, small bubbles and water droplets contributed significantly to the aeration process, and a sensitive probe is essential to accurately obtain the interfacial properties. Basically detection of microscopic bubble sizes requires a sensor size smaller than the bubbles, complemented by a high scanning frequency that gives a scanning resolution on the order of magnitude of the sensor tip.

Acknowledgments

Notation

The following Symbols are used in this paper:

a = specific interface area (m⁻¹) defined as air–water surface area per unit volume of air and water;

a_{mean} = average interface area (m⁻¹) in cross section of fluid normal to flow direction;

C = void fraction, or air concentration, defined as volume of undissolved air per unit volume of air and water;

C_{DS} = downstream dissolved gas concentration (kg/m^3);

C_{gas} = dissolved gas concentration (kg/m^3);

C_{mean} = cross-sectional averaged void fraction;

C_{SAT} = dissolved gas saturation concentration in water (kg/m^3);

C_{US} = upstream dissolved gas concentration (kg/m^3);

d = water depth (m);

d_c = critical flow depth (m);

d_t = tailwater depth (m);

d_0 = inflow depth (m);

E = aeration efficiency;

$E_{cascade}$ = aeration efficiency of stepped channel;

$E_{overfall}$ = aeration efficiency of free overfall;

E_{system} = aeration efficiency of system (multistepped chanel plus overfall);

F = bubble count rate (Hz) defined as number of bubbles impacting probe sensor per second;

F = Froude number;

F_0 = inflow Froude number;

H = total head (m);

H_{dam} = dam or weir height (m);

h = vertical step height (m);

K_L = liquid film coefficient (m/s);

L_{CASC} = stepped chute length (m);

L_D = free jet drop length (m);

n = constant;

q_w = water discharge per unit width (m^2/s);

T = water temperature;

t = time (s);

V = air–water velocity (m/s);

V_{mean} = average air–water flow velocity (m/s);

V_0 = inflow velocity (m/s);

W = channel width (m);

X = dimensionless longitudinal coordinate: $X = x/d_0$;

x = longitudinal coordinate (m), positive in downstream direction;

Y = dimensionless transverse coordinate: $Y = 2y/W$;

y = transverse coordinate (m), measured from channel centerline;

Z = dimensionless vertical coordinate: $Z = z/d_0$;

z = vertical coordinate (m), positive upwards;

z_{90} = vertical distance (m) where $C = 0.90$;

ϕ_a = air-bubble diameter (m); and

$\varnothing$ = diameter (m)

Subscript

$\circ$ = inflow conditions.

References

American Public Health Association, American Water Works Association, and Water Pollution Control Federation (APHA/AWWA/WPCF). (1989). *Standard methods for the examination of water and wastewater*, 7th Ed..

Apted, R. W., and Novak, P. (1973). "Oxygen uptake at weirs." *Proc., 15th IAHR Congress*, Vol. 1, Istanbul, Turkey, 177–186.

Avery, S. T., and Novak, P. (1978). "Oxygen transfer at hydraulic structures." *J. Hydraul. Div., Am. Soc. Civ. Eng.*, 104(11), 1521–1540.

Barrett, M. G., Gameson, L. H., and Ogden, C. G. (1960). "Aeration studies at four weir systems." *Water Water Eng.* September, 407–413.

Butts, T. A., and Evans, R. L. (1983). "Small stream channel dam aeration characteristics." *J. Environ. Eng.*, 109(3), 555–573.

Chanson, H. (1997). "Measuring air–water interface area in supercritical open channel flow." *Water Res.*, 31(6), 1414–1420.

Chanson, H. (2001). *The hydraulics of stepped chutes and spillways*, Balkema, Lisse, The Netherlands.

Chanson, H. (2002). "Air–water flow measurements with intrusive, phase-detection probes: Can we improve their interpretation?." *J. Hydraul. Eng.*, 128(3), 252–255.

Chanson, H., and Toombes, L. (2002). "Experimental study of gas-liquid interfacial properties in a stepped cascade flow." *Environ. Fluid Mech.*, 2(3), 241–263.

Department of the Environment (1973). "Aeration of weirs." *Notes on water pollution*, No. 61, Water Research Lab., Elder Way, Stevenage, Herts, U.K.

Department of Scientific and Industrial Research (DSIR). (1957). "Oxygen balance in surface waters." *Water pollution research*, DSIR, U.K., 12–21.

Essery, I. T. S., Tebbutt, T. H. Y., and Rasaratnam, S. K. (1978). "Design of spillways for reaeration of polluted waters." *CIRIA Rep. No. 72*, January, London.

Foree, E. G. (1976). "Reaeration and velocity prediction for small streams." *J. Environ. Eng. Div. (Am. Soc. Civ. Eng.)*, 102(5), 937–952.

Gameson, A. L. H. (1957). "Weirs and the aeration of rivers." *J. Inst. Water Eng.*, 11, 477–490.

Gulliver, J. S. (1990). "Introduction to air–water mass transfer." *Proc., 2nd Int. Symp. on Gas Transfer at Water Surfaces*, Air–Water Mass Transfer, S. C. Wilhelms and J. S. Gulliver, eds., ASCE, Minneapolis, 1–7.

Holler, A. G. (1971). "The mechanism describing oxygen transfer from the atmosphere to discharge through hydraulic structures." *Proc., 14th IAHR Congress*, Vol. 1, Paper A45, Paris, 372–383.

Kawase, Y., and Moo-Young, M. (1992). "Correlations for liquid-phase mass transfer coefficients in bubble column reactors with Newtonian and non-Newtonian fluids." *Can. J. Chem. Eng.*, 70, 48–54.

Mastropiertro, M. A. (1968). "Effects of dam reaeration on waste assimilation capacities of the Mohawk River." *Proc., 23rd Industrial Waste Conf.*, Engineering Extension Series, No. 132, Part 2, Purdue Univ., West Lafayette, Ind., 754–765.

Nakasone, H. (1987). "Study of aeration at weirs and cascades." *J. Environ. Eng.*, 113(1), 64–81.

Tebbutt, T. H. Y. (1972). "Some studies on reaeration in cascades." *Water Res.*, 6, 297–304.

Tebbutt, T. H. Y., Essery, L. T. S., and Rasaratnam, S. K. (1977). "Reaeration performance of stepped cascades." *J. Inst. Water Eng.*, 31(4), 285–297.

Toombes, L. (2002). "Experimental study of air-water flow properties on low-gradient stepped cascades." PhD thesis, The Univ. of Queensland, Queensland, Australia.

Watson, C. C., Walters, R. W., and Hogan, S. A. (1998). "Aeration performance of low drop weirs." *J. Hydraul. Eng.*, 124(1), 65–71.